

**Correlative Analysis of Hard and Soft X-ray
Emissions in Solar Flares**

-97-
NASA / CR-203898

FINAL REPORT

S-57783-F

IN-92-CR

1993 000410

Submitted to:

NASA/GSFC Greenbelt, MD 20771

Submitted by:

Dominic M. Zarro
Applied Research Corporation,
8201 Corporate Dr. Landover, MD 20785.

Date:

May 20, 1997

1. INTRODUCTION

This report describes research performed under the Phase 5 *Compton Gamma-Ray Observatory (CGRO)* Guest Investigator Program. The objective of this work is to study different mechanisms of solar flare heating by comparing their predictions with simultaneous hard and soft X-ray observations. The datasets used in this work consist of hard X-ray observations from the *CGRO* Burst and Transient Source Experiment (BATSE) and soft X-ray observations from the Bragg Crystal Spectrometer (BCS) and Soft X-ray telescope (SXT) on the Japanese *Yohkoh* spacecraft.

2. WORK PERFORMED

Research focussed on developing methods for determining the thermodynamic conditions in solar flares in which DC-electric field acceleration is responsible for producing impulsive non-thermal hard X-ray emission. The plasma temperature and density are two critical parameters that affect the efficiency of runaway acceleration. In particular, under low density and high temperature conditions, electron runaway acceleration is expected to dominate as a greater fraction of thermal electrons have sufficiently large velocities to undergo runaway. With increasing density, such as would occur during chromospheric evaporation, collisional redistribution inhibits the runaway process by thermalizing these high velocity electrons. Hence, in order to overcome this density “quenching” effect and sustain the production of nonthermal electrons by runaway acceleration, the electron temperature within the acceleration region must increase significantly during the flare. The following analysis presents a method for deducing the temperature in the acceleration region by combining simultaneous *Yohkoh* soft X-ray and *CGRO* BATSE hard X-ray obseravations, and comparing the results with measurements of “super-hot” temperatures in solar flares.

DC-electric fields and their associated electric currents have been shown to provide a viable mechanism for heating plasma and accelerating electrons in solar flares (Tsuneta 1985, Holman 1985). We deduce the temperature in the acceleration region by solving the energy balance equation in a 1-dimensional loop consisting of field-aligned currents. The energy balance equation is expressed as,

$$dU/dt = Q - R - dF_c/dz - 5nkTdv/dz, \quad (1)$$

where $U = 3nkT$ is the thermal energy per unit volume, Q is the total flare heating rate, $F_c \simeq -10^{-6}T^{5/2}dT/dz$ is the Spitzer conductive heat flux, $R \simeq an^2T^{-1/2}$ is the optically thin cooling rate, and the velocity gradient term is the enthalpy flux of evaporative motions within the loop.

We model the loop as a two-component plasma consisting of current-heated flux tubes with total volume V_f (in which electrons are runaway-accelerated), and a surrounding volume V_s which is not directly heated by currents but is in thermal and pressure equilibrium with the current-heated plasma. Such “filamentation” of the loop plasma is expected from electrodynamic arguments. In

particular, for a loop current system to remain stable, the total induction magnetic field strength of current-carrying electrons (drifting and accelerated electrons) must be less than that of the ambient coronal magnetic field (Holman 1985).

We represent the temperature and density within each filament by T_f and n_f , and the corresponding values in the surrounding plasma by T_s and n_s , respectively. The density and temperature within the filamento and surrounding regions are assumed to be uniform along the loop length. This approximation is expected to become valid approximately 20–30 s after heating onset when conduction will have redistributed the heat energy throughout the loop, and hydrodynamic motions will have restored approximate pressure balance within the loop (Fisher 1989). Accordingly, we simplify equation (1) by spatially averaging it with respect to the total loop volume $V (= V_f + V_s)$ such that,

$$\dot{U}_f V_f + \dot{U}_s V_s = Q_f V_f - R_f V_f - R_s V_s \quad (2),$$

where Q_f is the heating rate within the filaments. The enthalpy and conductive terms vanish at the loop apex and are negligible in the chromosphere ($z = 0$) relative to the heating and cooling terms. From pressure-balance, $T_f n_f = T_s n_s$, which implies $U_s = U_f$ and which further reduces the energy balance equation to,

$$\dot{U}_s V = Q_f V_f - R_f V_f - R_s (V - V_f) \quad (3).$$

The filament heating rate consists of a Joule heating term given by,

$$Q_{curr} = n_f k T_f \nu_e (E/E_D)^2 \quad \text{ergs cm}^{-3} \text{ s}^{-1} \quad (4)$$

where $\nu_e \approx 3.2 \times 10^2 n_f T_f^{-3/2} \text{ s}^{-1}$ is the thermal collision frequency (for classical resistivity), E is the electric field strength (assumed uniform along the loop length), and $E_D = 7 \times 10^{-8} n_f T_f^{-1}$ volts cm $^{-1}$ is the Dreicer field (Dreicer 1959). The Dreicer field is the field strength at which all the electrons in the current filaments plasma undergo thermal runaway. The heating rate also contains a Coulomb heating term due to accelerated electrons that propagate along the flare loop. For a power-law spectrum of electrons, the loop-integrated collisional heating rate assuming thick-target electrons is approximated by (Lin and Hudson 1976),

$$Q_{elec} = 1.6 \times 10^{-9} \gamma (\gamma - 1)^{-1} E_c \dot{N} \quad \text{ergs s}^{-1} \quad (5),$$

where,

$$\dot{N}_{thick} \simeq 3 \times 10^{33} a_1 (\gamma - 1)^2 B(\gamma - 1/2, 1/2) E_c^{-\gamma} \quad \text{s}^{-1} \quad (6),$$

is the total number flux of nonthermal electrons, a_1 and $\gamma = \delta - 1$ are the amplitude and spectral index, respectively, for a power-law approximation to the nonthermal hard X-ray spectrum

produced by the electrons, and E_c is the low-energy cutoff of the electron energy spectrum. For electrons produced by runaway acceleration the number flux is given by,

$$\dot{N}_{run} \simeq .35n_c v_e (E_D/E)^{3/8} \exp[-2^{1/2}(E_D/E)^{1/2} - (1/4)(E_D/E)] V_f \quad s^{-1} \quad (7),$$

which includes electrons that are accelerated out of the thermal distribution as well as electrons that are scattered into the runaway regime by collisions (Holman 1985).

Substituting the above heating terms into the energy balance equation we obtain,

$$\dot{U}_s V = Q_{curr} V_f + Q_{elec} - R_f V_f - R_s(V - V_f) \quad (8).$$

The energy balance equation consists of 4 unknowns: T_f , n_f , V_f , and E . We eliminate n_f by using pressure balance to relate the temperature and density within individual current filaments to the corresponding values in the larger surrounding loop volume such that $n_f = T_s n_s / T_f$. We eliminate V_f by equating the thick-target electron flux (eq. 6) with the theoretical electron runaway flux (eq. 7). The energy balance equation is thus reduced to the two unknowns T_f and E and the quantities V , T_s , and n_s , which are constrained by observations. In particular, we equate the total loop volume with the observed loop volume $V = 2AL$, where A is the observed loop area and L is the loop half-length. We infer T_s from soft X-ray observations of the thermal plasma using the temperature-sensitive Ca XIX resonance line (§ 3), and n_s from the Ca XIX emission measure $EM \approx n_s^2 V_s$.

3. RESULTS

The energy balance equation could not be solved uniquely for E and T_f without an additional constraining relation between these two parameters. One approach is to exploit the relationship between the critical energy for runaway acceleration and the electron low-energy cutoff E_c . The critical energy separates thermal and runaway electrons and is given by $E_{crit} = m_e v_f^2 / 2$ where v_f is the threshold velocity above which thermal electrons exceed frictional forces and runaway (Benka 1991, Benka and Holman 1992). This threshold velocity is given by $v_f = (E_D/E)^{1/2} v_e$ where $v_e = 2kT_f/m_e^{1/2}$ is the electron thermal velocity. Setting $E_c = E_{crit}$, we derive $E/E_D = E_c/(2kT_f)$. Substituting the latter into equation (8), we can solve for T_f for different specified values of E_c that are assumed constant during the flare. In this manner, we produce a grid of (T_f, E_c) solutions as a function of time during the flare.

We applied this technique to three flares that were observed simultaneously by *CGRO* BATSE and *Yohkoh* BCS and SXT. The first flare was an M1.9 event that occurred at 15:40 UT on 1992 February 17 (Kucera *et al.* 1996). The second was an M3.3 event that occurred at 09:00 UT on 1992 September 6 (Zarro, Mariska, and Dennis 1995). The third event was the famous impulsive loop-top flare that occurred at 17:27 UT on 1992 January 13 (Masuda 1993). For each flare we used SXT Beryllium filter images obtained at the onset of the hard X-ray impulsive phase to determine the characteristic soft X-ray loop volume. We determined the electron temperature

and plasma emission measure from least-squares fits of synthetic spectra to the Ca XIX resonance and dielectronic lines observed with the BCS. Figure 1 shows a sample fitted Ca XIX spectrum for the September flare.

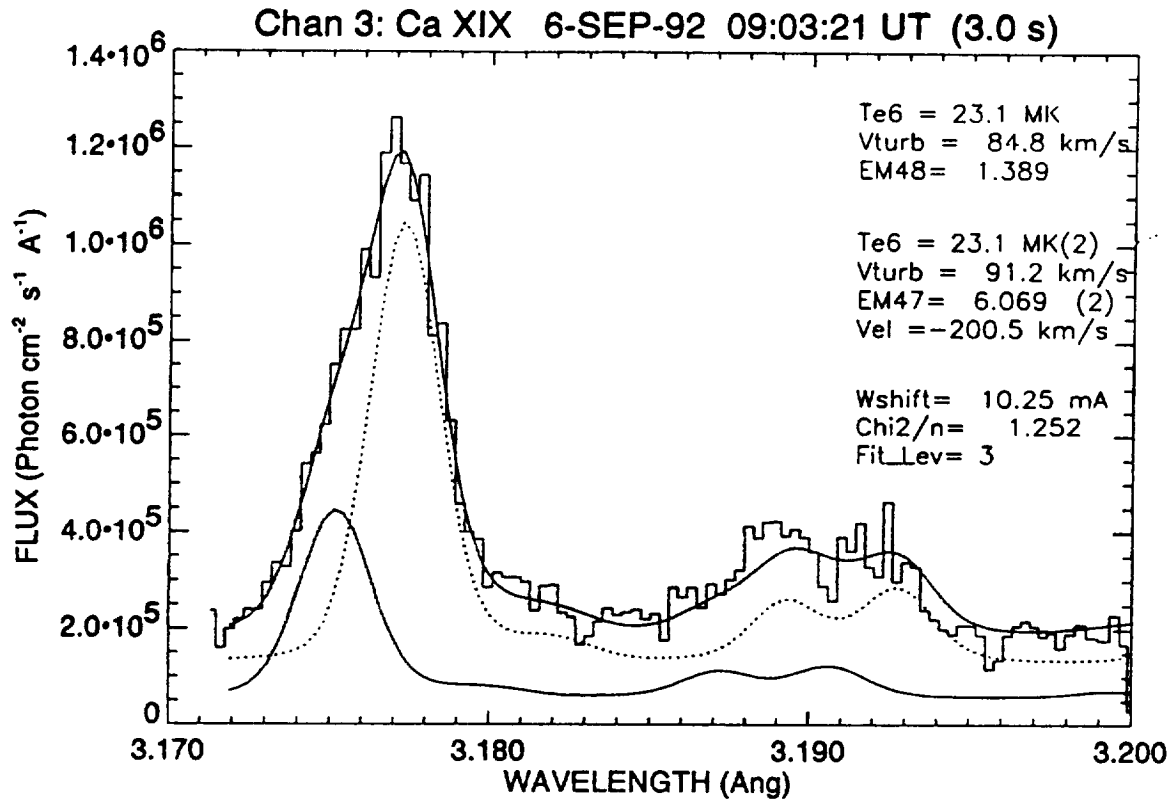


Figure 1. A two-component fit to the *Yohkoh*/BCS Ca XIX spectrum for the 1992 September 6 flare. The fit yields the temperature, emission measure (hence, density), and velocity upflow for the flare thermal component.

We used the BATSE LAD Continuous data to derive the nonthermal hard X-ray parameters of each flare. This data type produces hard X-ray spectra in 16 channels between 10 and > 1000 keV at 2.048 sec temporal resolution. We modelled the deconvolved LAD spectra in the 20-100 keV range with a power-law function of the form $I = a_1 \epsilon^{-\gamma}$ and used a least-squares fitting technique to infer a_1 and γ . Figure 2 shows a sample fitted power-law spectrum for one of the LAD flare intervals.

We developed Interactive Data Language (IDL) code to iteratively solve equation (8) for times when overlapping BCS and BATSE data were available. Generally, the signal-to-noise in both datasets was optimum during the main hard X-ray emission phase. Hard and soft X-ray fluxes were typically too weak during the early rise phase to produce reliable spectral fits. During

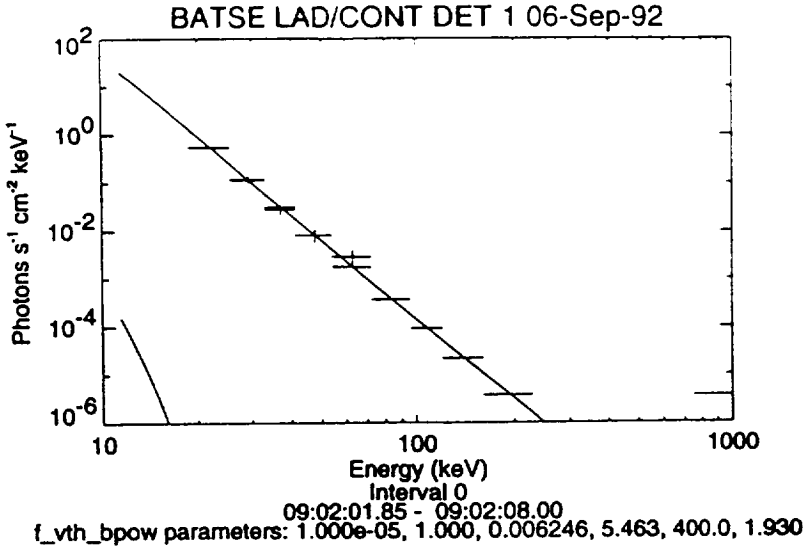


Figure 2. Power-law fit to the BATSE LAD CONT spectrum at the time of the first hard X-ray burst for the flare observed on 1992 September 6

this initial rapid heating phase, the assumptions of uniform temperature and density are not applicable. We created a grid of constant low-energy cutoff models ranging between $E_c = 10$ and 50 keV, in steps of 5 keV. For each E_c , we solved equation (8) for the variation of T_f using the empirical values of a_1 , γ , T_s , n_s , and V .

For all three events, we found that no solutions could be obtained for values of E_c below 30 keV. For these “low” cutoff energies, the implied number flux of nonthermal thick-target electrons (eq. 6), exceeded the predicted flux of runaway electrons (eq. 7) by orders of magnitude. For $E_c > 30$ keV, several temperature solutions were found that yielded agreement between observed and predicted electron fluxes. Figure 3 illustrates these solutions for the 13 January and 17 February flares for selected values of E_c . The computed loop filament temperatures are compared with the Ca XIX-soft X-ray temperatures, and with simultaneous measurements of the “super-hot” temperature component derived from fits of a thermal bremsstrahlung model to low-energy (< 20 keV) hard X-ray emission. In each flare, the Ca XIX-inferred temperatures (which are associated with the non-current heated loop region) were considerably cooler than T_f . In the case of the 13 January flare, the super-hot temperature was derived from the BATSE high resolution spectroscopy detector (SD) which consists of 256 channels. Figure 4 shows a sample fit of a bremsstrahlung plus power-law component to one of the SD flare intervals. The super-hot temperatures varied in the range $33 - 38 \times 10^6$ K, which matched closely the filament temperature variation corresponding to $E_c = 35$ keV. For the 17 February event, the super-hot temperature was derived by Kucera *et al.* (1996) using the L (15-24 keV) and M1 (24-35 keV) channel ratios of the *Yohkoh* Hard X-ray Telescope. Although the super-hot temperature correlated closely with the overall variation of T_f , it could not be matched by a single value of E_c , but instead with

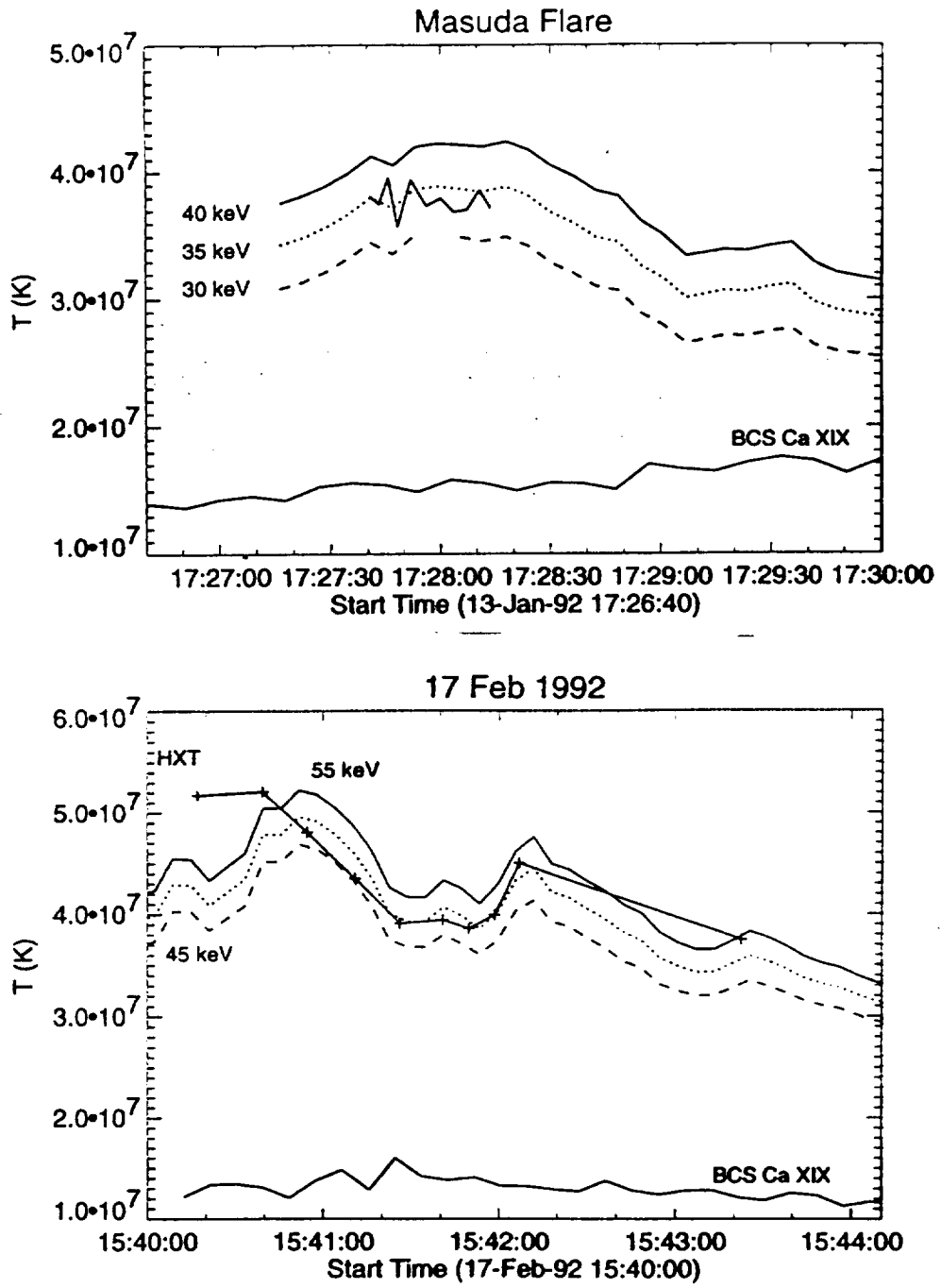


Figure 3. Loop filament temperatures T_f (smooth labelled curves) computed for different electron low-energy cutoff E_c values in the 13 January (upper panel) and 17 February (lower panel) flares. Shown for comparison are the cooler Ca XIX-inferred temperatures which are associated with the non-current heated loop plasma, and the “super-hot” HXR-inferred temperatures which are associated with the current heated regions.

values of E_c in the range 45–55 keV.

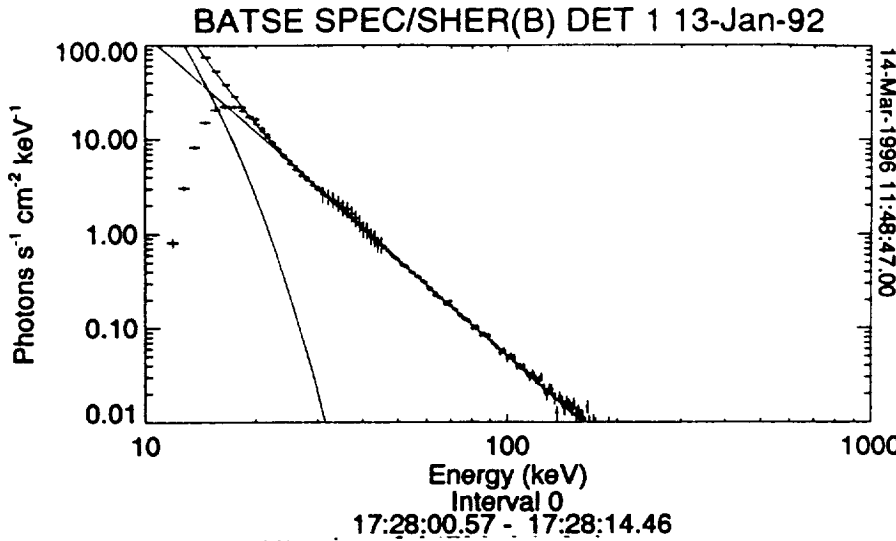


Figure 4. Thermal bremsstrahlung plus power-law fit to the BATSE Spectral Detector SHERB spectrum at the time of the first hard X-ray burst for the flare observed on 1992 January 13

4. SUMMARY

The main conclusion of our work is that the DC-electric field heating and acceleration model can explain the thermal and nonthermal properties of solar flares in a manner consistent with energy balance. In order for the model to self-consistently explain thermal soft X-ray emission and nonthermal hard X-ray emission, our simple energy balance calculations indicate that a “super-hot” component must exist within the flaring loop. This “super-hot” component is necessary to ensure a sufficient supply of thermal electrons to offset the collisional thermalization that occurs when the density within the loop increases because of chromospheric evaporation. The “super-hot” region is associated with a current-heated region that is cospatial with the electron runaway-acceleration region. In our analysis, the “super-hot” component arises in filamentary structures that extend along the length of a coronal loop in which Joule current-heating and runaway electron acceleration occur simultaneously. The observation of hard X-rays in footpoints with opposite magnetic polarity, suggest that a fraction (50 %) of the total number of filaments must have electric field components that are directed in opposite directions.

REFERENCES

- Benka, S.G. 1991, Ph.D. Thesis, Univ. of North Carolina, Chapel Hill
- Benka, S.G., and Holman, G.D. 1992, ApJ, 391, 854
- Dreicer, H. 1959, Phys. Rev., 115, 238
- Fisher, G.F. 1989, ApJ, 346, 1019
- Holman, G.D. 1985, ApJ, 293, 584
- Holman, G.D., Kundu, M., and Kane, S. 1989, ApJ, 345, 1050
- Kucera, T.A., Love, P.J., Dennis, B.R., Holman, G.D., Schwartz, R.A., and Zarro, D.M. 1996, ApJ, 466, 1067
- Lin, R.P.. and Hudson, H.S. 1976, Solar Phys., 50, 153
- Masuda, S. 1993, PhD Thesis, University of Tokyo
- Tsuneta, S. 1985, ApJ, 290, 353
- Zarro, D.M., Mariska, J.T., and Dennis, B.R. 1995, ApJ, 440, 888

Energetic Consequences of the DC-Electric Field Model

Dominic M. Zarro

Applied Research Corporation, NASA/GSFC Code 682.3, Greenbelt,
 MD 20771, USA

Richard A. Schwartz

Hughes/STX, NASA/GSFC Code 682.3, Greenbelt, MD 20771, USA

We created a desaturated set of full-frame images (FFI) from series of long

and short exposure. These images were then used to make the SXT movie. From the movie inspection we can see that there is a big loop (C in Figure 3) present from the first FFI inspected, i.e., from 17:24 UT till at least 21:00 UT.

3. Conclusion

It is suggested that the "spotless" flare studied in this paper was a consequence of both, 1) the large-scale restructuring of the magnetic field taking place in the solar corona, and 2) emerging magnetic flux. The flare was found to occur in the reversed sector as seen in a magnetic field synoptic chart (SGD) of the computed coronal magnetic field (Antalová, 1994 and references therein). The flare site was located close to the neutral line on the source surface ($r=2.5$ solar radii). It is suggested that the gradual magnetic reversal of the large-scale magnetic field of the Sun can inhibit activity in the lower parts of the solar atmosphere. Further study is in progress.

Acknowledgments. The H-alpha data were kindly made available by Dr. D. Neidig of NSO/Sac Peak. Thanks are also due to the British Council in Prague for financial support.

References

- Antalová, A. 1994, in proc. IAU Coll. 144, V. Rusin, P. Heinzel, and J.-C. Vial (eds.), VEDA Publ. House, Bratislava, 263-266
- Moore, R. L. 1995, ApJ, 438, 985
- Solar Physical Data, U.S. Dept. of Commerce, NOAA, Boulder, Colorado

Abstract. We analyze a solar flare observed simultaneously in soft and hard X-rays by instruments onboard *Yohkoh* and the *Compton Gamma Ray Observatory*. Assuming a simple one-dimensional coronal loop that is heated by field-aligned currents, we solve the energy balance equation to derive the DC-electric field strength necessary to explain the observed soft X-ray emission by current-dissipation. We use the derived DC-electric field to predict the number flux of electrons accelerated by thermal runaway and compare this prediction with the number flux of nonthermal thick-target electrons implied by impulsive phase hard X-ray observations. We find that runaway acceleration can account for the large flux ($\gtrsim 10^{36} \text{ s}^{-1}$) of nonthermal electrons provided the loop filling factor is $\lesssim 10^{-3}$ such that heating and acceleration occur in filamented structures within the loop.

1. Introduction

Magnetic field line reconnection models predict DC-electric field components parallel to the loop magnetic field (Tsuneta 1995). It has been proposed that such DC-electric fields can produce nonthermal electrons in solar flares via thermal runaway acceleration (Tsuneta 1985, Holman 1985). In particular, a DC-electric field will accelerate thermal electrons until a steady state current is established. Since the collisional drag on the electrons decreases with increasing velocity, those electrons with velocities above a critical velocity will undergo runaway acceleration producing nonthermal electrons that emit hard X-ray radiation via thick-target interactions (Holman, Kundu, and Kane 1989). Electrons below the runaway threshold continue to heat the loop plasma producing soft X-ray emission. This paper investigates the energetics of the DC-electric field model by examining whether the DC-electric field strength implied by soft X-ray heating is sufficient to account for the number flux of nonthermal electrons implied by hard X-ray observations.

In the following section, we derive the DC-electric field strength by solving the energy balance equation in a single loop with uniform cross-sectional area. As input to this equation, we use simultaneous soft and hard X-ray observations from *Yohkoh* and the *Compton Gamma Ray Observatory (CGRO)* of a

simple loop flare that occurred on 1992 September 6. From the *Yohkoh* Soft X-ray Telescope (SXT), we infer the geometry of the flaring loop. From the *Yohkoh* Bragg Crystal Spectrometer (BCS), we derive the temperature T and emission measure EM of the flare source. From the CGRO Burst and Transient Spectrometer Experiment (BATSE), we deduce the number flux of accelerated electrons.

2. Method

For a one-dimensional loop, the energy balance equation is expressed as

$$\frac{dU}{dt} = Q - R - \frac{dF_c}{dz} - 5nkT \frac{dv}{dz}, \quad (1)$$

where $U = 3nkT$ is the thermal energy per unit volume, Q is the total flare heating rate, $F_c \simeq -10^{-6}T^5/dT/dz$ is the Spitzer conductive heat flux, $R \simeq anT^{-1/2}$ is the optically thin cooling rate, and the velocity gradient term is the enthalpy flux of convective motions within the loop. For the radiative cooling coefficient, we use $a = 2.2 \times 10^{-19}$ which is based on calculations by Raymond, Cox, and Smith (1976). We shall assume that the density n and temperature T are uniform along the loop length. This assumption is valid about 20–30 s after heating onset when thermal conduction will have redistributed the heat energy throughout the loop, and hydrodynamic motions will have restored approximate pressure balance within the loop (Fisher and Hawley 1990).

We simplify equation (1) by spatially averaging it with respect to the total loop volume such that

$$\dot{U}V = QV_c - RV + [5nkTv(0) + F_c(0)]A, \quad (2)$$

where V is the total volume of the loop and V_c is the volume of the current-heated region. The enthalpy and conductive fluxes vanish at the loop apex and are negligible in the chromosphere ($z = 0$) relative to the heating and radiative cooling terms. Note that the volume of the current-heated region is assumed to be less than the total observed loop volume $V = 2AL$, where A is the observed loop area and L is the loop half-length. From the ratio of these two volumes, we define a filling factor $f = V_c/V$. Following Holman (1985), we assume that the heat energy generated within each current channel is distributed into the larger loop volume by conductive (or convective) transport processes on a timescale less than the heating timescale.

For a loop that is heated uniformly by current-dissipation, the Joule heating rate is given by

$$Q_{curr} = nkT\nu_e(E/E_D)^2 \quad \text{ergs cm}^{-3} \text{ s}^{-1}, \quad (3)$$

where $\nu_e \approx 3.2 \times 10^2 nT^{-3/2} \text{ s}^{-1}$ is the thermal collision frequency (for classical resistivity), E is the electric field strength (assumed uniform along the loop length), and $E_D = 7 \times 10^{-8}nT^{-1}$ volts cm^{-1} is the Dreicer field. The Dreicer field is the field strength at which all the electrons in the plasma undergo thermal runaway. Substituting Q_{curr} into equation (2), we derive the following analytic expression for E

$$E = E_D \sqrt{\frac{(U + R)}{fnkT\nu_e}} \quad (4)$$

Given n and T , we solve equation (4) for the variation of E during the flare for different values of the filling factor. Given E , we can subsequently compute the rate of runaway electrons assuming that runaway acceleration occurs within the same current-heated channels. The runaway rate is given by the formula

$$\dot{N}_{run} \simeq 35n\nu_e(E_D/E)^{3/8} \exp[-2^{1/2}(E_D/E)^{1/2} - (1/4)(E_D/E)]V_c \quad \text{s}^{-1}, \quad (5)$$

which includes electrons that are accelerated out of the thermal distribution as well as electrons that are scattered into the runaway regime by collisions (Kruskal and Bernstein 1964). The runaway electrons that propagate along the loop will heat the plasma by Coulomb collisions, producing thick-target hard X-ray emission as they impact the chromosphere. Assuming a power-law electron energy spectrum with spectral index δ above a low-energy cutoff E_c , the total number flux of hard X-ray-producing electrons is given by

$$N_{thick} \simeq 3 \times 10^{33} a_1 (\gamma - 1)^2 B(\gamma - 1/2, 1/2) E_c^{-\gamma} \quad \text{s}^{-1}, \quad (6)$$

where $B(x, y)$ is the beta function, $\gamma = \delta - 1$ is the power-law spectral index, and a_1 is the power-law amplitude, respectively, of the emitted hard X-ray spectrum (Lin and Hudson 1976). The low-energy cutoff is determined by the critical energy above which thermal electrons exceed the frictional force and undergo thermal runaway. The critical energy is given by $E_{crit} = m_e(E_D/E)v_e^2/2$, where v_e is the electron thermal velocity (Holman 1985).

3. Results

We apply equation (4) to an M3.3 flare that was observed by *Yohkoh* and *CGRO* at 09:00 on 1992 September 6 (Zarro, Mariska, and Dennis 1995). From least-squares fits of synthetic spectra to the BCS Ca XIX (λ 3.177 Å) resonance line, we obtain the variations of T and EM . From preflare SXT images, we infer a loop half-length $L \simeq 3 \times 10^9 \text{ cm}$, a loop cross-sectional area $A \simeq 3 \times 10^{17} \text{ cm}^2$, and a total observed volume $V \simeq 2 \times 10^{27} \text{ cm}^3$. From the emission measure and filling factor, we derive the loop density $n \simeq (EM/fV)^{1/2}$. Substituting into equation (4), we compute E for different values of f .

Figure 1 shows the time variation of E for $f = 0.1, 0.01$, and 0.001 . The DC-electric field strength increases with decreasing filling factor. This effect occurs because the density within the current channels is inversely proportional to f . Consequently, since $U \sim n$, a higher electric field strength is required to sustain the enhanced heating rate within the channels. Similarly, the electric field strength increases with time during the flare rise phase because the density within the current channels increases as plasma is heated and evaporated into the loop.

We use the BATSE LAD Continuous data to derive the nonthermal parameters of the flare. This data type produces hard X-ray spectra in 16 channels

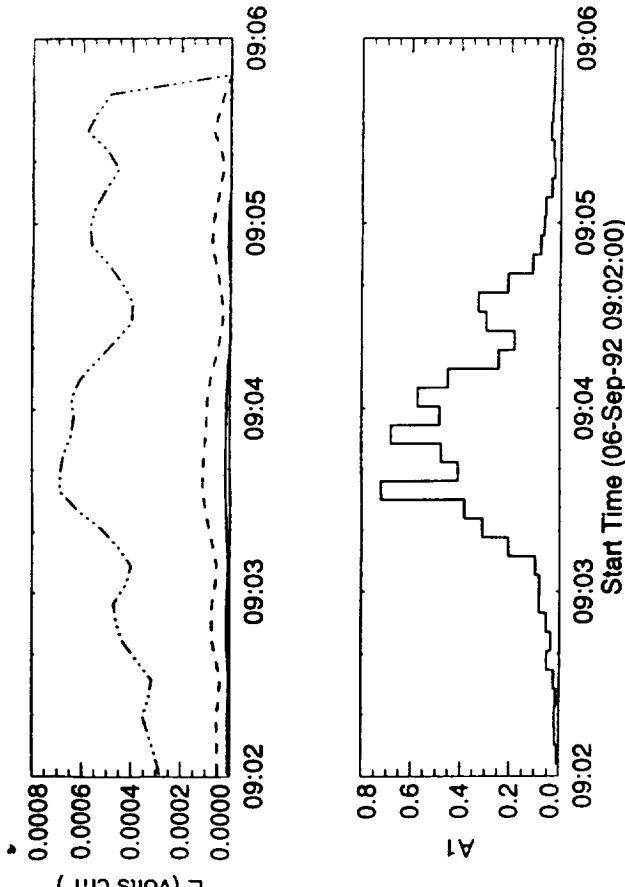


Figure 1. Upper Panel: Variation of DC-electric field strength for filling factors $f = 0.1$ (solid), 0.01 (dash), and 0.001 (dash-dot). Lower Panel: Fitted power-law amplitude of nonthermal hard X-ray emission.

between 10 and > 1000 keV at 2.048 sec temporal resolution. The spectra show a well-defined power-law distribution of the form $I = a_1 \epsilon^{-\gamma}$ in the 20-100 keV range. From a least-squares deconvolution of the LAD response function, we obtain the temporal variations of the amplitude a_1 and spectral index γ of the power-law component. The variation of a_1 is compared with E in Figure 1. The temporal variations of these quantities are correlated such that the maximum DC-electric field coincides with the peak of hard X-ray burst emission.

For each filling factor, we use the derived values of E to compute the number flux of nonthermal electrons from the thick-target equation (6) and compare it with the number flux predicted by the runaway formula (5). Figure 2 shows his comparison for $f = 0.001$. The latter filling factor yields the optimum agreement between the measured and predicted fluxes during the rise phase of impulsive hard X-rays. For this filling factor, the peak DC-field strength is 3×10^{-4} volts cm $^{-1}$, giving a peak runaway flux of 3×10^{37} s $^{-1}$. Such a high flux is a direct consequence of the low cutoff energy ($E_c \approx 10$ keV) implied by the critical energy for thermal runaway.

For $f > 0.001$, runaway acceleration alone does not produce sufficient nonthermal electrons to match the observed flux. In this case, the density within the current-heated region is too low to provide a large enough population of thermal electrons to undergo runaway. For $f < 0.001$, runaway acceleration also fails to match the observed number flux. Examination of equation (5), shows

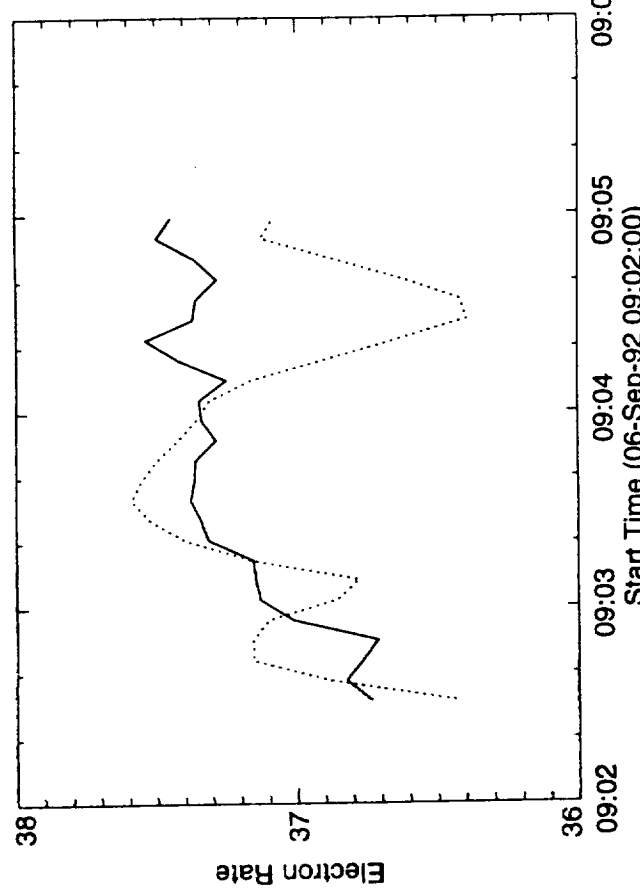


Figure 2. Comparison between the number flux of nonthermal electrons implied by hard X-ray observations (solid) and the number flux predicted by runaway acceleration for a volume filling factor of 0.001 (dashed).

that $N_e^{\text{run}} \sim \exp(-E_D/E)$. Since $E_D \sim n$, the runaway rate drops exponentially with increasing density. Physically, the runaway electrons become thermalized by collisions when the density in the current-heated region becomes very large.

The predicted and observed electron fluxes show a large discrepancy after hard X-ray maximum ($\approx 09:04$ UT) and cannot be reconciled with any value of f . This discrepancy reflects a breakdown in many of the simplifying assumptions that underly the energy-balance analysis. First, the assumption of a filling factor that is constant in time is likely to become invalid as the flare energy is distributed throughout the loop system and the heating extends to possibly multiple loops. Second, the assumption that the hard X-ray emission is predominantly nonthermal (and thick-target in origin) becomes questionable when the temperature within the heated region becomes very high and the apparent power-law spectrum is actually the result of a strong thermal bremsstrahlung component. The present soft and hard X-ray observations cannot distinguish this case.

4. Conclusions

We conclude from energy balance that DC-electric field heating and acceleration can self-consistently explain thermal soft X-ray emission and nonthermal

The Maximum Temperatures of Flare Thermal Plasma and Their Implication

T. Watanabe
*National Astronomical Observatory, 2-21-1 Osawa, Mitaka,
 Tokyo 181, Japan*

$$V_j \lesssim \frac{LB^2}{4\pi n^2 e^2} \left(\frac{c}{v_e} \right)^2 \left(\frac{E_D}{E} \right)^2, \quad (7)$$

where B is the loop magnetic field strength. To satisfy this constraint, the acceleration region must be fragmented into $n_c = V_c/V_j$ multiple filaments. Adopting a typical loop field strength of $B = 100$ Gauss, and using the value of E computed at hard X-ray maximum for $f = 0.001$, we deduce a peak $n_c \simeq 10^{12}$. The existence of such a large number of current filaments introduces serious problems for maintaining charge-neutrality in the loop plasma. One possible solution is that the current systems are closed by cross-field drifting of protons at the chromospheric footpoints (Emslie and Henoux 1995).

References

- Fisher, G., & Hawley, S. 1990, *ApJ*, 357, 243
- Holman, G. 1985, *ApJ*, 293, 584
- Holman, G., Kundu, M., & Kane, S. 1989, *ApJ*, 345, 1050
- Emslie, A. G., & Henoux, J.-C. 1995, *ApJ*, 446, 371
- Kruskal, M., & Bernstein, I. 1964, *Phys. Fluids*, 7, 407
- Lin, R., & Hudson, H. 1976, *Solar Phys.* 50, 153
- Raymond, J.C., Cox, D.P., & Smith, B.W. 1976, *ApJ*, 204, 290
- Tsuneta, S. 1985, *ApJ*, 290, 353
- Tsuneta, S. 1995, *PASJ*, 47, 691
- Zarro, D., Mariska, J., & Dennis, B. 1995, *ApJ*, 440, 888

Extended Abstract

The investigation of diagnostic characteristics in small flares is important for clarifying whether the solar flare is a homogeneous energy release process.

The same method as in the previous papers is used in the present analysis (Watanabe et al. 1992, 1995). In order to derive electron temperatures, the line-ratio method is adopted. Total intensities of the resonance line (w), of the blended feature with the dielectronic satellites (j and k) and the forbidden line (z) are obtained by integrating 13 bins around the line centers. The ratio gives the electron temperature in the coronal condition of low-density limit. Preflare background intensities, mainly coming from active regions and quiet-sun, are subtracted (Watanabe et al. 1992, 1995) in the analysis.

The maximum temperature increases slightly with flare intensity, though Watanabe (1994) concluded that it was constant. In the current data set, including the samples of Watanabe (1994), the relationship of

$$\log [T_{e,\max}] = (0.080 \pm 0.008) \times \log [\text{GOES flux}(1-8\text{\AA})] + \text{const.},$$

is obtained. The power index of the maximum emission measure against the soft X-ray intensity (*GOES*) is 0.788 ± 0.021 , somewhat flatter than unity.

The thermal property of flare plasmas is uniform in five orders of magnitude in soft X-ray intensity. The solar flare is a very homogeneous phenomenon at least in this energy range, and heating in flares is also a universal process to produce roughly similar shapes of the differential emission measure (DEM) in flare thermal plasmas.

References

- Watanabe, T. 1994, in Proc. *Kofu Symp. New Look at the Sun with Emphasis on Advanced Observations of Coronal Dynamics and Flares*, eds. Enome, S. and Hirayama, T., NRO Rep. 360, 99
- Watanabe, T., Hiei, E., Lang, J., Culhane, J. L., Bentley, R. D., Doschek, G. A., Bromage, B. J. I., Brown, C. M., Feldman, U., Fludra, A., Kato, T., and Payne, J. 1992, *Publ. Astron. Soc. Japan*, 44, L141
- Watanabe, T., Hara, H., Shimizu, T., Hiei, E., Bentley, R. D., Fludra, A., Lang, J., Phillips, K. J. H., Pike, C. D., Bromage, B. J. I., and Mariska, J. T. 1995, *Solar Phys.*, 157, 169

REPORT DOCUMENTATION PAGE

*Form Approved
OMB No. 0704-0188*

Public reporting burden for this collection of information is estimated to average 1 hour per response, including the time for reviewing instructions, searching existing data sources, gathering and maintaining the data needed, and completing and reviewing the collection of information. Send comments regarding this burden estimate or any other aspect of this collection of information, including suggestions for reducing this burden, to Washington Headquarters Services, Directorate for Information Operations and Reports, 1215 Jefferson Davis Highway, Suite 1204, Arlington, VA 22202-4302, and to the Office of Management and Budget, Paperwork Reduction Project (0704-0188), Washington, DC 20503.

1. AGENCY USE ONLY (Leave blank)			2. REPORT DATE May 1997		3. REPORT TYPE AND DATES COVERED Contractor Report	
4. TITLE AND SUBTITLE Correlative Analysis of Hard and Soft X-ray in Solar Flares			5. FUNDING NUMBERS S-57783-F			
6. AUTHOR(S) Dr. Dominic Zarro			8. PERFORMING ORGANIZATION REPORT NUMBER R97-257			
7. PERFORMING ORGANIZATION NAME(S) AND ADDRESS (ES) Applied Research Corp. 8201 Corporate Drive, Suite 1120 Landover, MD 20785			9. SPONSORING / MONITORING AGENCY NAME(S) AND ADDRESS (ES) National Aeronautics and Space Administration Washington, DC 20546-0001			
10. SPONSORING / MONITORING AGENCY REPORT NUMBER CR-203898			11. SUPPLEMENTARY NOTES			
12a. DISTRIBUTION / AVAILABILITY STATEMENT Unclassified - Unlimited Subject Category: 90 Report available from the NASA Center for AeroSpace Information, 800 Elkridge Landing Road, Linthicum Heights, MD 21090; (301) 621-0390.				12b. DISTRIBUTION CODE		
13. ABSTRACT (Maximum 200 words) <p>We propose to continue a study that we have commenced under the Cycle 3 and 4 GI programs. Our broad aim is to test flare models by comparing their predictions with simultaneous BATSE hard x-ray and Yohkoh soft x-ray observations. For Cycle 5, we will focus on the hydrodynamic consequences of current heating and runaway acceleration. We will use BATSE spectra in the 20–300 keV range from the Large Area detectors to deduce the nonthermal hard x-ray component that is related to the electron heating rate. We will use Yohkoh soft x-ray data to deduce the thermal heating rate and the plasma cooling rates of the evaporating chromospheric component. By comparing these rates, we will place tighter constraints on the physical parameters that control heating and acceleration in solar flares.</p>						
14. SUBJECT TERMS Sun, Flares, Corona						15. NUMBER OF PAGES 13
						16. PRICE CODE
17. SECURITY CLASSIFICATION OF REPORT Unclassified	18. SECURITY CLASSIFICATION OF THIS PAGE Unclassified	19. SECURITY CLASSIFICATION OF ABSTRACT Unclassified	20. LIMITATION OF ABSTRACT UL			